Vibrational characterization of active drug to the treatment of chagas disease, benznidazole by using force fields and internal coordinates

Maximiliano A. Iramain (ID), María E. Manzur (ID), María V. Castillo (ID), María A. Checa (ID),
Elida Romano (ID), Silvia A. Brandán ✉ (ID)

Cátedra de Química General. Instituto de Química Inorgánica. Facultad de Bioquímica, Química y Farmacia.
Universidad Nacional de Tucumán. Ayacucho 471. T4000INI San Miguel de Tucumán. Tucumán. Argentina

Abstract:

Two experimental structures of benznidazole active drug used to the treatment of Chagas disease have been structurally characterized and its vibrational spectra completely assigned combining B3LYP/6-311++G** calculations with the experimental FT-IR and FT-Raman spectra and the SQMFF methodology. The most stable conformer of benznidazole found in the study of the potential energy surface is in agreement with that experimentally observed by X-ray diffraction at room temperature while the other one was observed with the heating up to 195 ºC. Both differs in the positions of CH_2 groups of acetamide fragment. Their structural properties in gas phase and ethanol solution were computed by using natural bond orbital (NBO), atoms in molecules (AIM), Merz-Kollman (MK) charges, molecular electrostatic potentials (MEP) and frontier orbitals calculations by using the hybrid B3LYP method and the 6-31G* and 6-311++G** basis sets. Additional WB97XD/6-311++G** calculations show that the energy values optimized for the most stable species in both media present lower values than the obtained with the B3LYP/6-31G* method. The vibrational assignments for those two conformers in both media were obtained from their corresponding harmonic force fields together with the scaled force constants.

Keywords: *Benznidazole, vibrational spectra, molecular structure, force field, DFT calculations.*

Introduction

The *N*-benzyl-2-(2-nitroimidazol-1-yl)acetamide compound, named benznidazole, is one active drug used during the first phase to the treatment of Chagas disease (Caryn, 2015; Rassi, Rassi, & Marin-Neto, 2010; Bern, 2015; Figueroa, et al., 2018; Tonin, et al., 2009; Soares-Sobrinho, et al., 2008; Nogueira Silva, et al., 2008; Soares-Sobrinho, et al., 2010; Pires, Hideki Yoshizane, & Souza, 2010; Pires, et al., 2011; Soares-Sobrinho, et al., 2012; Arancibia, et al., 2013; Bezerra, et al., 2014; Honorato, et al., 2014;

Arenas Velásquez, et al., 2014; Aguirre, et al., 2004; Trochine, et al., 2014; Olivera, et al., 2016; Streck, et al., 2016; Figueirêdo, et al., 2017; Morillo, et al., 2017). The cause of this illness in the humans is the parasite *Trypanosoma Cruzi*, as is largely known (Caryn, 2015; Rassi, Rassi, & Marin-Neto, 2010; Bern, 2015). There are a lot of studies of this interesting substance related to different chemical, physicochemical and biological properties and to preparations of new derivatives in order to obtain better bioactive species (Soares-Sobrinho, et al., 2010; Pires, Hideki Yoshizane, & Souza, 2010; Pires, et al.,

2011; Arancibia, et al., 2013; Arenas Velásquez, et al., 2014; Trochine, et al., 2014; Streck, et al., 2016; Figueirêdo, et al., 2017; Morillo, et al., 2017). Benznidazole has low solubility in water for which this drug is employed in combination with other species, such as complexes, in order to improve their solubility and efficacy, as reported by different studies (Figueroa, et al., 2018; Tonin, et al., 2009; Nogueira Silva, et al., 2008; Soares-Sobrinho, et al., 2010; Pires, et al., 2011; Figueirêdo, et al., 2017). The experimental benznidazole structure was determined by using X-ray diffraction by Soares-Sobrinho et al. while their new polymorphs structures were elucidated by Honorato et al. by using the same technique (Soares-Sobrinho, et al., 2008; Honorato, et al., 2014). Previously, the theoretical structures of benznidazole were studied by Tonin et al. and, recently, two conformations were reported for this species by Oliveira et al. in order to investigate the intra-molecular hydrogen bonds in their structures (Tonin, et al., 2009; Olivera, et al., 2016). These authors have optimized two structures of benznidazole in aqueous solution which are the *s-cis* and *s-trans* forms by using the B3LYP/6-311++G(d,p) method and the PCM model (Olivera, et al., 2016). Those two conformations can be seen in Figure 1.
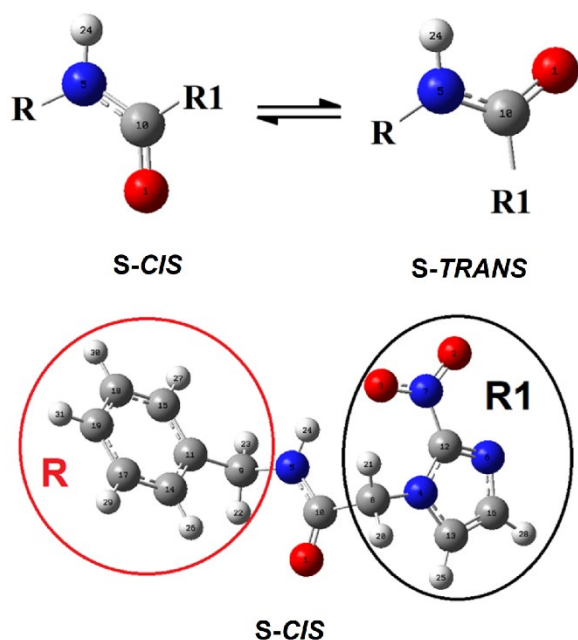
**Figure 1. Conformations s-*cis* and s-*trans* of Benznidazole**

The physicochemical characterization of benznidazole by using the infrared and Raman spectra and the studies of thermal stability and compatibility were also performed by Soares-Sobrinho et al. but in this study the vibrational assignments of both spectra for benznidazole were no reported (Soares-Sobrinho, et al., 2010). Obviously, the complete characterization of this important drug by using the vibrational spectroscopy is very important to identify with this technique their presence in different media. Hence, the aims of this work are to perform the complete assignments of the vibrational spectra for those two experimental structures observed of benznidazole combining DFT calculations with the experimental infrared and Raman spectra by using their harmonic force fields, normal internal coordinates, transferable scaling factors and the SQMFF methodology (Pulay, et al., 1983; Rauhut, & Pulay, 1995; Sundius, 2002). For these purposes, the potential energy surfaces for conformations *cis* and *trans* of benznidazole were studied in gas phase and in ethanol solution by using the B3LYP/6-31G(d) and 6-311++G(d,p) and WB97XD methods (Becke, 1988; Lee, Yang, & Parr, 1988; Chai, & Head-Gordon, 2018) while the solvent effects in solution were considered with the polarized continuum (PCM) and solvation models (Tomasi, & Persico, 1994; Miertus, Scrocco, & Tomasi, 1981; Marenich, Cramer, & Truhlar, 2009). Here, our results suggest two stable *cis* conformers for benznidazole, named C2 and C4, where the assignments of both forms *s-Cis* were considered in the vibrational analyses because only these structures were experimentally observed by X-ray diffraction although C4 was observed not at room temperature as C2 (Soares-Sobrinho, et al., 2008; Honorato, et al., 2014). At this time, the structural, topological and vibrational properties were studied in both media for the most stable C2 structure of benznidazole observed at room temperature. Then, the harmonic scaled force constants for those structures of benznidazole in both media were reported for both methods. Additionally, the frontier orbitals were used to predict their reactivities and behaviours in both media by using different global descriptors (Parr, & Pearson, 1983; Karrouchi, et al., 2021; Laurella,

et al., 2022; Karrouchi, et al., 2021; Mortada, et al., 2022).

Computational Approaches

The *GaussView* and Gaussian 16 programs were used to model and optimize the initial benznidazole (BENZ) structure by using the hybrid B3LYP and WB97XD methods and the 6-31G* and 6-311++G** basis sets (Dennington, Keith, & Millam, 2019; Frisch, et al., 2019). Later, the potential energy surfaces (PES) described by the dihedral N4-C8-C10-N5, C11-C9-N5-C10, C8-C10-N5-C9 angles were studied with those levels of theory and only the graphic for the dihedral C11-C9-N5-C10 angle by using the 6-31G* basis set is presented in Figure 2.
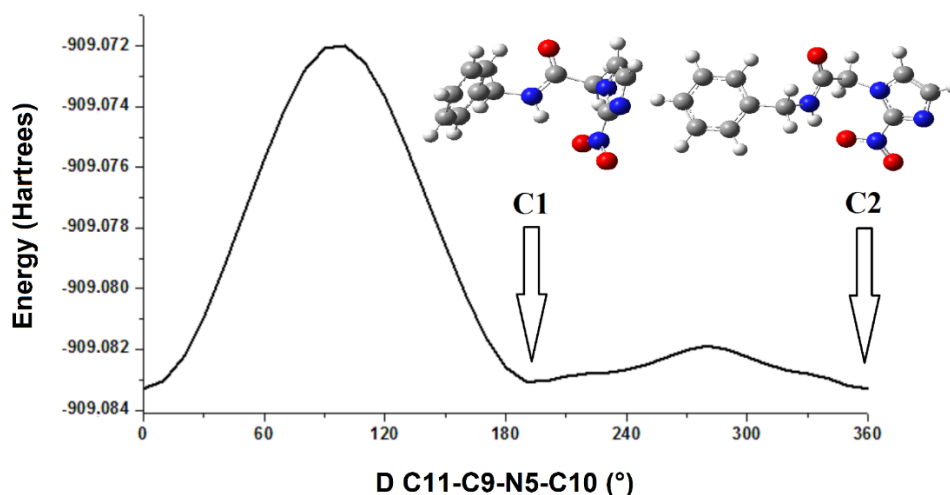
Figure 2. Potential Energy Surfaces (PES) for Benznidazole Described by the Dihedral C11-C9-N5-C10 Angle by Using the B3LYP/6-311++G Method**

Figure 2 shows only two stable conformations which are named C1 and C2 while the C3 *trans* form is unstable due to steric hindrance of both R and R1 groups and, also to the repulsions between closer N and O atoms. Then, taking into account that the experimental structure of benznidazole reported by Soares-Sobrinho et al. is different from that published by Braga Honorato et al., other C4 form *Cis* of BENZ was studied at the same level of theory (Soares-Sobrinho, et al., 2008; Honorato, et al., 2014). Between both structures only changes in the positions of two CH$_2$ groups linked to benzyl and acetamide fragment are observed with the heating, as mentioned by Honorato et al. (Honorato, et al., 2014). However, the optimizations of C4 in both media show that this structure is the same than C2 but with opposite dihedral angles. Thus, for the C2 conformation experimentally observed, atomic natural population (NPA) and Merz-Kollman (MK)

charges were studied in the two media (Besler, Merz, & Kollman, 1990). Moreover, the molecular electrostatic potentials were calculated by using those latter charges while the donor-acceptor interactions and bond orders were computed by using NBO calculations (Glendening, et al., 1996). Intra-molecular interactions were evaluated taking into account the atoms in molecules theory by using the topological properties calculated with the AIM2000 program (Bader, 1990; Biegler-Köning, Schönbohm, & Bayles, 2001). In this work, the frontier orbitals were first calculated and, then, the gap values and, after that, with these values the chemical potential (μ), electronegativity (χ), global hardness (η), global softness (S) and global electrophilicity index (ω) descriptors were predicted by means of know equations (Parr, & Pearson, 1983; Karrouchi, et al., 2021; Laurella, et al., 2022; Karrouchi, et al., 2021; Mortada, et al., 2022). Harmonic force

fields and the scaled force constants were determined with the SQMFF methodology and the Molvib program using normal internal coordinates and transferable scaling factors (Pulay, et al., 1983; Rauhut, & Pulay, 1995; Sundius, 2002) while in the vibrational assignments of IR and Raman spectra we considered potential energy distribution (PED) contribution $\geq 10\%$. Further, the ^{1}H and ^{13}C chemical shifts were computed applying the Gauge-Independent Atomic Orbital (GIAO) method using tetramethylsilane (TMS) as reference (Ditchfield, 1974). Here, Time-dependent DFT calculations (TD-DFT) at the B3LYP/6-311++G** levels of theory were applied to predict the ultraviolet-visible spectrum of BENZ in ethanol solution using the Gaussian 16 program (Frisch, et al., 2019). In addition, the TDDFT calculations were also employed to predict the rotatory strengths by ECD.

Results and Discussion

Structural Study

First, B3LYP/6-31G* calculations were performed for BENZ, three *s-CIS* (C1, C2 and C4) and one *s-TRANS* named C3 and, then, hybrid B3LYP/6-311++G** calculations in order to analyse the populations of those conformers of BENZ. Hence, a comparison of theoretical C2 and C4 structures of BENZ with the corresponding experimental at room temperature determined by X-ray diffraction by Soares-Sobrinho et al (Soares-Sobrinho, et al., 2008) and by Honorato et al with the heating (Honorato, et al., 2014) are shown in Figure 3.
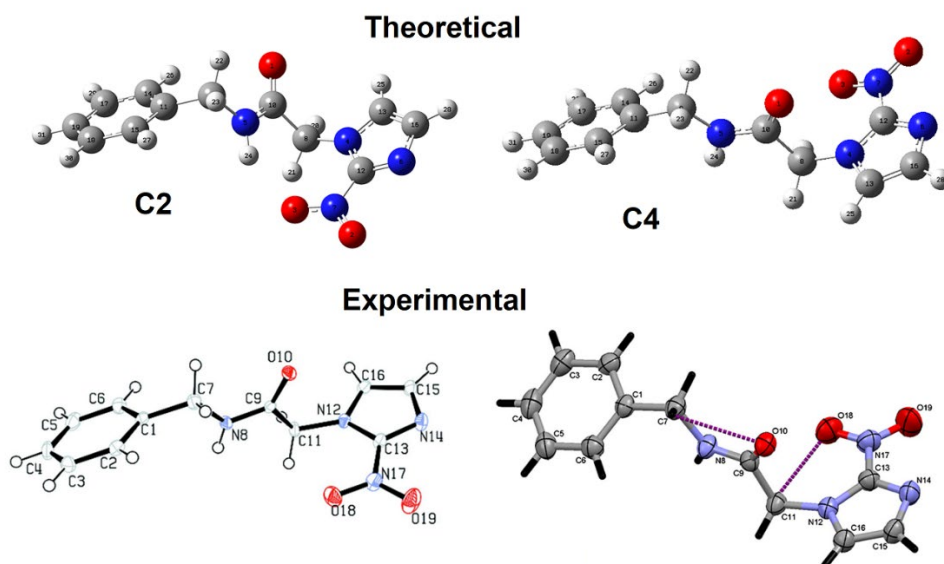
Figure 3. Comparisons Between the Theoretical C2 and C4 molecular structures of benznidazole with the corresponding experimental determined respectively at room temperature and with the heating
Source: Soares-Sobrinho, et al., 2008; Honorato, et al., 2014

Then, total and relative energies, dipolar moment, volume and population values for those conformers of BENZ calculated in the two media with both B3LYP and WB97XD methods and the 6-311++G** basis set are shown in Table 1. Two dihedral C11-C9-N5-C10 and N4-C8-C10-N5 angles are also included in that table together with the populations.

Table 1. Calculated Total (E) and Relative Energies (ΔE), Dipole Moments, Molecular Volume and Populations (%) for the Most Stable Conformers of Benz in Both Media and at Different Levels of Theory

Forms	E (Hartrees)	μ (Debye)	V (Å³)	ΔE (kJ/mol)	Population (%)	Dihedral angles (º)	
						C11-C9-N5-C10	N4-C8-C10-N5
GAS PHASE							
B3LYP/6-311++G**							
s-CIS							
C1	-909.3392	2.50	262.7	0.00	35.58	-93.9	-88.8
C2	-909.3390	2.93	264.7	0.52	28.84	107.9	-86.8
C4	-909.3392	2.50	267.8	0.00	35.58	95.1	89.8
s-TRANS							
C3	-909.3320	7.45	265.2	18.88	0.00	124.4	-165.2
ETHANOL SOLUTION							
s-CIS							
C1	-909.3761	11.56	271.1	0.00	35.58	-111.2	-159.6
C2	-909.3761	11.69	276.0	0.00	35.58	112.5	-159.9
C4	-909.3759	11.61	262.3	0.52	28.84	112.2	160.4
WB97XD/6-311++G**							
Gas	-909.0311	2.38	261.1	-	-	96.5	-76.3
Ethanol	-909.0682	11.41	258.8	-	-	95.8	-161.9

Regarding Table 1, we observed that the energy values of C1 and C2 with both methods are approximately similar between them but with differences of 0.52 kJ/mol in gas phase. The energy, V, μ and population values for both in solution with the B3LYP/6-311++G** method are the same and the only difference observed between them is the positive C11-C9-N5-C10 dihedral angle. Then, C1 structure is the same than C4 in gas phase but this latter structure is observed with the heating while C2 is observed at room temperature. Thus, the only structure experimentally observed at room temperature is C2. Besides, the C4 form in gas phase is different from the optimized in solution, as can be seen in Figure S1 (Appendix 1). Table 1 also shows that C3 structure presents the higher relative energy (18.88 kJ/mol) and dipole moment in gas phase by using the B3LY/6-311++G** level of theory and, consequently, null population is observed in both media. Hence, taking into account that C2 is the only conformer experimentally observed at room temperature, the properties for this form of BENZ were predicted by using the higher level of theory. Additional WB97XD/6-311++G** calculations have optimized C2 in gas phase with an E value of -909.0311 Hartrees and μ= 2.38 D. An E value enough lower than the obtained with the B3LYP/6-31G* method

in the same medium (-909.0831 Hartrees), as reported for other species (Sundius, & Brandán, 2023; Romano, E., et al., 2023). When the dipole moment values for the C1, C2, C3 and C4 conformers in gas phase are graphically represented by using the B3LYP/6-311++G** method we observed that the magnitudes, directions and orientations of their vectors are different among them, as shown in Figure S2 (Appendix 1). In C1, C2 and C4 the vectors are oriented in direction to C=O bonds on to acetamide fragment while in C3 the vector is located within the CH$_2$ group near to benzyl ring, as observed in Figure S2 (Appendix 1). Probably, the positions, directions and orientations of dipole moments vectors and, their magnitudes explain the presence of C2 in the solid phase, as was reported for other compounds (Romano, et al., 2011; Romano, et al., 2013; Romano, Ladetto, & Brandán, 2013; Guzzetti, et al., 2013). Apparently, these results could have impact on structural and electronic properties and, on its reactivities and behaviours in both media.

Theoretical geometrical parameters calculated for C2 in both media using two B3LYP methods with the 6-31G* and 6-311++G** basis sets are compared in Table 2 with the corresponding experimental determined by X-ray diffraction by

Soares-Sobrinho et al (2008). Here, the predicted parameters with the WB97XD method were not considered because the E values obtained are lower than the B3LYP/6-31G* level of theory. The differences between these data are expressed by means of root-mean-square deviation (RMSD). In general, we observed good correlations in the bond lengths for the C2 structures with both methods with values between 0.122 and 0.078 Å but a better agreement is observed for C2 in gas phase with the B3LYP/6-311++G** method while for the bond angles similar correlations are observed with both methods (2.9-2.7°). Probably, the good correlations observed for bond lengths and angles could explain why C2 is the conformation experimentally observed. However, great variations are observed in the dihedral angles because some angles change theirs values and signs in ethanol solution. These calculations show changes in the different dihedral angles related to the imidazole and benzyl rings and to acetamide fragment in gas phase and in ethanol solution but a very important observation for C2 in the two media and with both methods is the similarity in the RMSDs values of dihedral angles. Thus, the values decrease from 209.4/208.4° in gas phase to 179.5/179.3 in solution. Hence, due to the presence of donor N-H group and of acceptors N and O atoms in the structure of BENZ could also be expected H bonds interactions in solution, as the strong intermolecular N-H⋯O hydrogen bonds observed in the crystal packing of BENZ in the solid phase (Soares-Sobrinho et al, 2008).

Table 2. Comparison of Calculated Geometrical Parameters for C2 of Benz in Gas Phase and Ethanol Solution by Using Different Levels of Theory with the Corresponding Experimental Ones

Parameters	B3LYP/*method[a]				EXP[a]
	6-31G		6-311++G**		
	GAS	Ethanol	GAS	Ethanol	
Bond lengths (Å)					
O1-C10	1.226	1.233	1.222	1.232	1.228
O2-N7	1.221	1.234	1.214	1.230	1.226
O3-N7	1.249	1.241	1.242	1.236	1.231
N4-C8	1.469	1.460	1.470	1.461	1.462
N4-C12	1.378	1.373	1.378	1.373	1.362
N4-C13	1.369	1.363	1.369	1.361	1.358
N5-C9	1.464	1.462	1.464	1.462	1.467
N5-C10	1.353	1.347	1.352	1.342	1.328
N5-H24	1.014	1.014	1.012	1.012	0.836
N6-C12	1.317	1.322	1.312	1.319	1.314
N6-C16	1.358	1.358	1.357	1.355	1.362
N7-C12	1.436	1.422	1.442	1.423	1.434
C8-C10	1.544	1.534	1.543	1.532	1.527
C8-H20	1.090	1.093	1.088	1.532	0.99
C8-H21	1.088	1.089	1.085	1.088	0.99
C9-C11	1.517	1.517	1.516	1.516	1.527
C9-H22	1.093	1.093	1.090	1.090	0.990
C9-H23	1.095	1.094	1.093	1.092	0.990
C11-C14	1.402	1.403	1.400	1.400	1.387
C11-C15	1.398	1.399	1.396	1.397	1.396
C13-C16	1.382	1.385	1.380	1.384	1.370
C13-H25	1.080	1.080	1.077	1.078	0.950

C14-C17	1.393	1.394	1.391	1.393	1.391
C14-H26	1.087	1.087	1.085	1.085	0.950
C15-C18	1.397	1.398	1.395	1.396	1.391
C15-H27	1.088	1.087	1.085	1.085	0.950
C16-H28	1.081	1.081	1.078	1.078	0.950
C17-C19	1.397	1.399	1.395	1.396	1.383
C17-H29	1.086	1.087	1.084	1.084	0.950
C18-C19	1.394	1.395	1.392	1.393	1.384
C18-H30	1.086	1.087	1.084	1.084	0.950
C19-H31	1.086	1.087	1.084	1.084	0.950
RMSD[a]	**0.080**	**0.080**	**0.078**	**0.122**	
Bond angles (°)					
C8-N4-C12	131.6	130.3	131.7	130.6	130.6
C8-N4-C13	123.3	124.4	123.3	124.1	124.1
C12-N4-C13	104.9	105.1	104.8	105.1	104.9
C9-N5-C10	122.4	123.7	123.0	124.4	121.0
C9-N5-H24	119.3	117.5	118.9	117.3	119.9
C10-N5-H24	118.0	118.6	117.9	118.2	118.2
C12-N6-C16	104.7	104.6	105.0	104.9	103.7
O2-N7-O3	124.3	123.7	124.5	123.6	124.0
O2-N7-C12	117.9	118.0	118.1	118.2	118.3
O3-N7-C12	117.6	118.1	117.3	118.0	117.6
N4-C8-C10	111.3	111.5	111.3	112.3	110.8
N4-C8-H20	107.5	106.7	107.2	106.6	109.5
N4-C8-H21	108.6	109.7	108.9	109.7	109.5
C10-C8-H20	107.0	108.4	106.9	108.0	109.5
C10-C8-H21	112.2	111.8	112.4	111.5	109.5
H20-C8-H21	109.9	108.3	109.8	108.3	108.1
N5-C9-C11	113.4	113.1	113.0	113.1	110.8
N5-C9-H22	106.2	106.4	106.4	107.0	109.5
N5-C9-H23	108.0	108.4	108.4	108.5	109.5
C11-C9-H22	110.5	110.7	110.6	110.5	109.5
C11-C9-H23	110.2	110.0	110.0	109.7	109.5
H22-C9-H23	108.0	107.7	108.0	107.6	108.1
O1-C10-N5	125.1	124.7	125.1	124.7	124.4
O1-C10-C8	120.1	121.3	119.9	121.4	120.9
N5-C10-C8	114.6	113.9	114.9	113.7	114.4
C9-C11-C14	120.1	120.4	120.2	120.8	120.4
C9-C11-C15	120.8	120.6	120.7	120.3	120.6
C14-C11-C15	119.0	118.8	118.9	118.8	118.9
N4-C12-N6	113.1	113.1	113.0	112.9	113.8
N4-C12-N7	124.2	123.9	124.3	124.0	123.4
N6-C12-N7	122.5	122.9	122.6	123.0	122.7
N4-C13-C16	106.5	106.6	106.6	106.8	106.7
N4-C13-H25	120.8	121.2	121.0	121.3	126.6
C16-C13-H25	132.5	132.0	132.2	131.7	126.6
C11-C14-C17	120.4	120.5	120.4	120.5	120.7

C11-C14-H26	119.2	119.5	119.4	119.7	119.6
C17-C14-H26	120.3	119.8	120.0	119.6	119.6
C11-C15-C18	120.6	120.6	120.6	120.6	120.4
C11-C15-H27	119.6	119.5	119.6	119.5	119.8
C18-C15-H27	119.7	119.8	119.6	119.7	119.8
N6-C16-C13	110.4	110.3	110.2	110.0	110.6
N6-C16-H28	121.5	121.9	121.6	122.1	124.7
C13-C16-H28	127.9	127.7	128.0	127.7	124.7
C14-C17-C19	120.1	120.1	120.1	120.1	119.7
C14-C17-H29	119.7	119.7	119.8	119.7	120.1
C19-C17-H29	120.0	120.0	120.0	120.0	120.1
C15-C18-C19	119.9	120.0	120.0	120.0	119.8
C15-C18-H30	119.8	119.7	119.8	119.7	120.1
C19-C18-H30	120.1	120.1	120.1	120.1	120.1
C17-C19-C18	119.7	119.6	119.7	119.6	120.2
C17-C19-H31	120.1	120.1	120.1	120.1	119.9
C18-C19-H31	120.1	120.2	120.1	120.2	119.9
RMSD[a]	**2.9**	**2.7**	**2.8**	**2.7**	
Dihedralangles (º)					
O2-N7-C12-N4	167.5	175.3	171.2	176.5	-5.0
O2-N7-C12-N6	-13.0	-4.8	-9.1	-4.6	177.1
O3-N7-C12-N4	-12.6	-4.9	-8.9	-3.7	174.1
O3-N7-C12-N6	166.8	174.8	170.6	175.0	-3.8
N7-C12-N4-C8	-1.0	0.2	-0.4	-2.1	5.8
N7-C12-N4-C13	178.9	179.1	179.2	178.7	-178.8
N7-C12-N6-C16	-178.9	-179.2	-179.1	-178.7	178.6
C12-N4-C8-C10	98.1	73.8	95.9	74.8	-97.7
N4-C8-C10-O1	101.2	23.5	92.5	22.6	20.4
N4-C8-C10-N5	-77.2	-158.8	-86.8	-159.9	-163.9
C8-C10-N5-C9	179.4	-173.9	179.0	-175.2	-176.5
C10-N5-C9-C11	93.5	107.1	107.9	112.5	167.8
O1-C10-N5-C9	1.0	3.5	-0.2	2.1	-1.0
RMSD[a]	**209.4**	**179.5**	**208.4**	**179.3**	

Note: [a]This work, [b] Soares-Sobrinho, et al., 2008
Source: Soares-Sobrinho, et al., 2008

NPA and MK Charges, MEP and Bond Orders

The interesting pharmacological properties observed in BENZ could probably be associated to the hydrophobic and hydrophilic sites and, for these reasons, the identifications of these possible reaction sites are necessaries requirements. Besides, the bond orders are related to forces of the different bonds and to those reactivity sites because when a bond is weak, the break of that bond is expected, so, for this reason, the bond order (BO) values is other very important property that must be studied. Hence, the atomic natural population (NPA), Merz-Kollman (MK) charges, molecular electrostatic potential (MEP) and bond orders (BO) values are investigate for C2 in both media (Besler, Merz, & Kollman, 1990). These three properties were analysed only for the acceptors (N and O atoms) and donors of H bonds (N-H) groups of BEZ in both media by using the B3LYP/6-311++G** method. Table 3

summarize those properties while Figure 4 shows the behaviours of two atomic charges studied on the atoms involved in acceptors and donor's groups of H bonds of C2. The exhaustive analysis of charges shows different curves indicating that the behaviours of MK charges are different from NPA ones. However, few changes are observed in both charges in ethanol solution.

Table 3. Atomic Natural Population (NPA), Merz-Kollman (MK) Charges, Molecular Electrostatic Potential (MEP) and Bond Orders (BO) Acceptors and Donor Groups of Most Stable C2 Conformer of BENZ in Gas Phase and Ethanol Solution by Using the B3LYP/6-311++G Levels of Theory**

Atoms	B3LYP/6-311++G** Method							
	MK		NPA		MEP		Bond Order	
	Gas	Ethanol	Gas	Ethanol	Gas	Ethanol	Gas	Ethanol
O1	-0.589	-0.732	-0.631	-0.729	-22.385	-22.423	1.984	1.871
O2	-0.397	-0.526	-0.318	-0.423	-22.323	-22.388	2.095	1.985
O3	-0.563	-0.550	-0.453	-0.430	-22.325	-22.353	1.962	1.983
N4	0.346	0.491	-0.387	-0.364	-18.281	-18.271	3.512	3.543
N5	-0.587	-0.489	-0.625	-0.603	-18.349	-18.323	3.268	3.287
N6	-0.497	-0.628	-0.424	-0.474	-18.377	-18.406	3.096	3.063
N7	0.794	0.803	0.464	0.470	-18.132	-18.165	3.967	3.965
H24	0.426	0.378	0.416	0.424	-1.003	-0.947	0.831	0.822

Note: Atomic charges and MEP values in a.u.
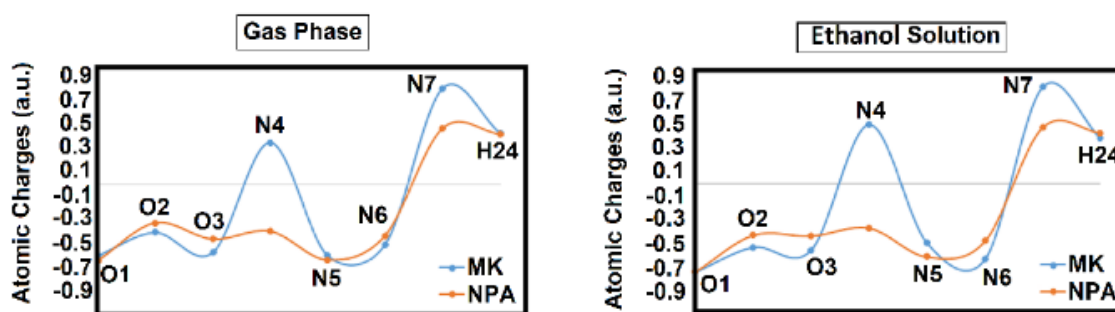
Figure 4. Variations Observed on Calculated MK and NPA Charges on N, O and H Atoms Corresponding to C2 of BENZ in Both Media by Using the B3LYP/6-311++G Method. N and O Atoms Belong to NO2 Group, to Imidazole and to Acetamide Fragment While the H Atom to NH Group.**

Regarding the two charges on O atoms, it is observed negative signs on three atoms but higher NPA values are observed on O2 and O3 of NO_2 groups in both media. On the other side, both charges on N5 and N6 show similar values in gas phase but their values change in solution while on N4 and N7 are observed positive MK and NPA charges but negative NPA charges only on N4 in the two media. Both charges on

H24 of donor N5-H24 group show similar positive values in the two media.

Analysing the MEP values from Table 3, we see the following tendency: O > N > H, as expected due to higher electronegativity of the O atom. Thus, in solution higher values are observed on three O atoms and N6 and N7 while lower values on N4 and N5. Probably, those increase in the MEP values on the atoms belonging to

C=O and NO₂ groups indicate hydration of these groups in solution while the lower MEP value observed on H24 indicate that this atom is the most labile because this atom belong to N-H group and, hence, it is clearly a donor of H bond. When the mapped MEP surface for C2 in gas phase is built with the *GaussView* program the nucleophilic and electrophilic regions are observed through the different colours, as shown in Figure 5 by using the different levels of theory (Dennington, Keith, & Millam, 2019).

B3LYP/6-31G*
±0.056 a.u.

B3LYP/6-311++G**
±0.054 a.u.
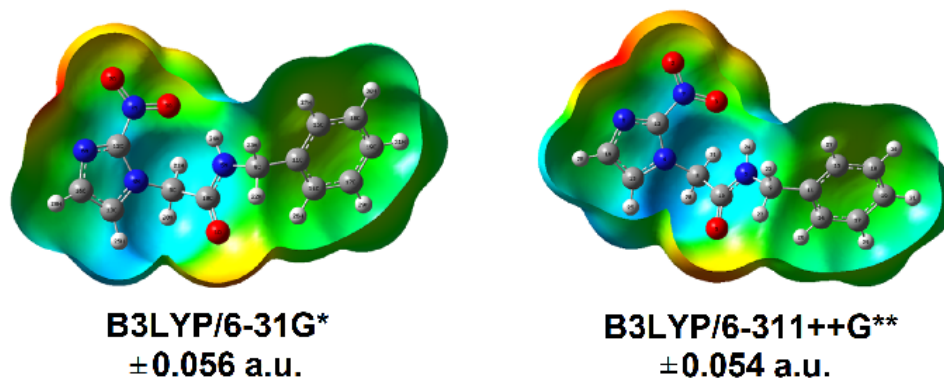
Figure 5. Calculated Electrostatic Potential Surfaces on the Molecular Surface of C2 of BENZ in Gas Phase by Using the Different Levels of Theory. Isodensity Value of 0.005.

From the figure 5 it is observed that the range colours decrease from ±0.056 a.u. with the B3LYP/6-31G* method to ±0.056 a.u. with the higher level of theory while the colorations observed in the different regions are approximately the same. Thus, the intense red colours are observed on the N6 of imidazole ring and on the O atoms of NO₂ and on C=O groups. These sites correspond to nucleophilic regions while the blue colours are observed on the N-H and CH₂ groups of acetamide fragment and correspond to electrophilic sites. In general, the green colours are observed on benzyl ring and correspond to inert sites.

In relation to the BO values, Table 3 show that the three O atoms and N6, N7 and H24 have lower values in solution while N4 and N5 present higher BO values in this medium. These variations in the BOs are related to their hydrations because they are clear sites of formation of H bonds.

Stability Studies

The stability study of BENZ is important due to its observed biological properties as a consequence of acceptors and donor's groups and, also because we need to know why C2 is

experimentally observed when the other stable C1 and C4 conformers have approximately the same energy values than C2 (Caryn, 2015; Rassi, Rassi, & Marin-Neto, 2010; Bern, 2015; Figueroa, et al., 2018; Tonin, et al., 2009). Hence, to examine the stabilities in both media NBO and AIM calculations were performed (Glendening, et al., 1996; Bader, 1990; Biegler-Köning, Schönbohm, & Bayles, 2001). Thus, the donor-acceptor energy interactions and their topological properties were predicted for C2 in both media and these results are presented in Tables S1 and S2 (Appendix 2), respectively (Glendening, et al., 1996). Regarding first the donor-acceptor energy interactions computed by using the two levels of theory from Table S1 (Appendix 2), we observed five different types of interactions: $\Delta ET_{\pi \to \pi*}$, $\Delta ET_{\pi \to LP}$, $\Delta ET_{\pi* \to \pi*}$, $\Delta ET_{LP \to \pi*}$ and $\Delta ET_{LP \to \sigma*}$ which are related to the double bonds of the benzyl ring (C=C), to the NH and NO₂ groups and to C=O bond of acetamide fragment. Besides, the lone pairs of the O and N atoms are clearly involved in the $\Delta ET_{\pi \to LP}$, $\Delta ET_{LP \to \pi*}$ and $\Delta ET_{LP \to \sigma*}$ interactions and present higher energy values in solution. In particular, the $\Delta ET_{\pi \to LP}$ interactions are predicted by the two methods only in ethanol

solution while the E values are strongly dependent on method and basis set because the *LP(1)N5→ σ*O1-C10, LP(1)N6→ π*N4-C12* and *LP(1)N6→π*C13-C16* interactions are only predicted in solution with the B3LYP/6-311++G** method. Thus, the evaluation of total energy with both methods show that C2 is most stable in solution (4683.20 kJ/mol) while in gas phase the higher stability is observed with the B3LYP/6-31G* level of theory (2900.57 kJ/mol).
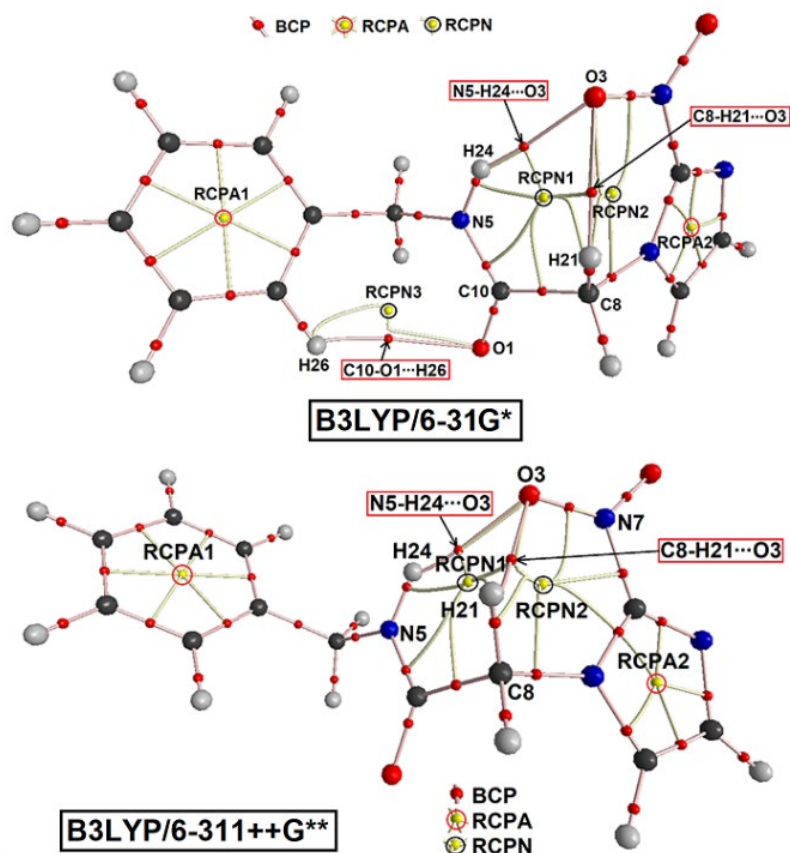

Figure 6. Details of the Molecular Model for the C2 Conformer of BENZ in Gas Phase by Using the B3LYP/6-31G*(Upper) and B3LYP/6-311++G** (Bottom) Levels of Theory
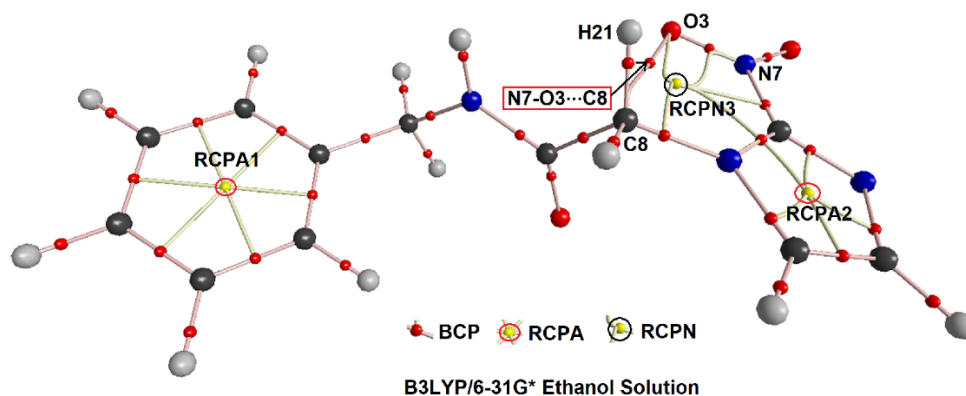

Figure 7. Details of the Molecular Model for the C2 Conformer of BENZ in Ethanol Solution by Using the B3LYP/6-31G* Level of Theory

The topological properties of C2 in the two media were also evaluated with the AIM 2000 program to predict their stabilities (Bader, 1990; Biegler-Köning, Schönbohm, & Bayles, 2001). Hence, the Bader's theory was used to analyse the intra-molecular interactions (Bader, 1990) calculating the electron density distribution, $\rho(r)$, the values of the Laplacian, $\nabla^2\rho(r)$, the eigenvalues $(\lambda 1, \lambda 2, \lambda 3)$ of the Hessian matrix and the $\lambda 1/\lambda 3$ ratio in the bond critical points (BCPs) and ring critical points (RCPs). Thus, with these parameters it is possible to identify the characteristics and type of interaction. Thus, when an interaction present high values of $\rho(r)$ and $\nabla^2\rho(r)$, the ratio $\lambda 1/\lambda 3 > 1$ and $\nabla^2\rho(r) < 0$ the interaction is covalent (shared interaction) while the interaction is ionic or highly polar covalent when $\lambda 1/\lambda 3 < 1$ and $\nabla^2\rho(r) > 0$ (closed-shell interaction). Hence, in Table S2 (Appendix 2) are summarized those parameters for C2 in both media while in Figure 6 can be seen details of the molecular models for the C2 conformer of BENZ in gas phase by using the B3LYP/6-31G* and B3LYP/6-311++G** levels of theory, respectively. The figure shows three H bonds interactions with the B3LYP/6-31G* method which are, N5-H24···O3, C8-H21···O3 and C10-O1···H26 interactions while with the higher level of theory only are predicted the two first interactions. Thus, Table S2 (Appendix 2) shows that the number of H bonds interactions and their properties are dependent on the used method. Analysing the interactions in ethanol solution with both methods from Figure 7 we observed for each method one same interaction but with different characteristics, as can be seen from Table S2 (Appendix 2). This way, Figure 7 shows the only N7-O3···C8 interaction predicted for both methods in solution by using the B3LYP/6-31G* method. A same graphic is observed with the other method and, for this reason, the corresponding figure is not presented here. Higher densities are predicted for the H bonds interactions in gas phase with the B3LYP/6-31G* method than the other one while on the contrary it is predicted for the RCPAs of rings and of new RCPNs.

The presence of three and two H bonds in C2 with both basis sets could justify its experimental presence in the solid phase. Note that RCPA1and RCPA2 belong to the benzyl and imidazole rings, respectively while the new ring critical points are identified as RCPN. Both NBO and AIM studies support the high stability of C2 conformer in the gas phase due to the presence of three different N-H···O, C-H···O and C-O···H interactions in gas phase and two in ethanol solution, as was observed in the crystal packing of BENZ in the solid phase (Soares-Sobrinho, et al., 2008). Besides, the high total energy value predicted by NBO analysis for C2 in ethanol solution using the B3LYP/6-311++G** method, as compared with the other one, reveal the influence of level of theory and the medium on the total stabilization energy.

Frontier orbitals and Descriptors

Reactivities and behaviours of C2 in gas phase and ethanol solution have been predicted by using the gap energy values calculated from the frontier orbitals, as suggested by Parr and Pearson (Parr, & Pearson, 1983). Then, with the gap values the chemical potential (μ), electronegativity (χ), global hardness (η), global softness (S) and global electrophilicity index (ω) descriptors were estimated using known equations (Karrouchi, et al., 2021; Laurella, et al., 2022; Karrouchi, et al., 2021; Mortada, et al., 2022; Sundius, & Brandán, 2023; Castillo, et al., 2018; Romano, E., et al., 2023). Thus, in Table S3 (Appendix 2) are summarized the gap values for C2 in the two media together with the calculated descriptors by using both levels of theory. The equations used in the calculations of descriptors are given in the same table. The results for C2 are compared with reported for the thiol and thione forms of 1,3-benzothiazole tautomers, a compound with potential antimicrobial activity because these species also present NO_2 groups in the five member's rings and have benzyl rings, as shown in Figure S3 (Appendix 1) (Romani, & Brandán, 2015). Regarding first the gap values for C2 with both methods, we observed that lower gap values are observed in solution, for which, C2 is most

reactive in solution. From the comparisons with the two tautomers of 1,3-benzothiazole, the thione form in gas phase is most reactive than C2 and thiol in the two media. Thus, the fused benzyl and thiazole rings increase the reactivity of compound. When the descriptors are evaluated we observed for the most reactive thiazole species < chemical potential (μ), < electronegativity (χ) and < global hardness (η). Thus, this study show that the different methods have few influence on the gap values and descriptors. Hence, the low gap values and the high reactivities of these species could explain their biological activities.

NMR Study

The predicted ^{1}H and ^{13}C NMR chemical shifts for C2 in ethanol solution were calculated for both levels of theory by using the GIAO method (Ditchfield, 1974) and are respectively compared in Tables 4 and **5** with the corresponding experimental ones for Benz in CHCl$_3$ taken from Ref (SpectraBase, n.a.) by using the RMSD values. In general, an overestimation in the theoretical values is observed with both methods as compared with the experimental ones and a better concordance for the ^{1}H nucleus (0.7 ppm) than for the ^{13}C nucleus (6.7-8.1 ppm) was observed.

Table 4. Observed and Calculated ^{1}H Chemical Shifts (δ in ppm) for BENZ in Ethanol Solution at Two Levels of Theory

	B3LYP Method		Exp
δ (ppm)	6-31G*	6311++G*	
H20	4.8	4.6	4.3
H21	5.1	5.0	4.3
H22	5.8	5.6	5.2
H23	3.9	3.8	3.4
H24	5.5	5.7	5.2
H25	7.3	7.3	7.4
H26	7.8	7.6	7.7
H27	7.5	7.5	8.6
H28	7.5	7.4	7.7
H29	7.8	7.7	8.7
H30	7.7	7.7	8.7
H31	7.7	7.6	8.7

RMSD	**0.7**	**0.7**	

Note: [a]This work, [b]From SpectraBase, (n.a.) for benz in CHCl$_3$

Table 5. Observed and Calculated ^{13}C Chemical Shifts (δ in ppm) for BENZ in Ethanol Solution at Two Levels of Theory

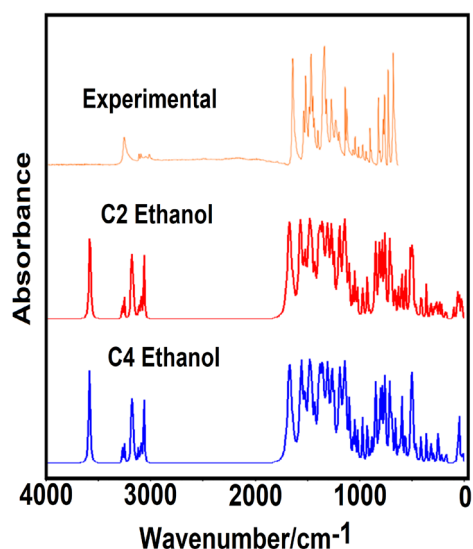|	B3LYP Method[a]		Exp[b]
δ (ppm)	6-31G*	6311++G**	
C8	63.9	56.6	53
C9	54.6	46.5	48
C10	166.5	172.0	164
C11	142.8	147.7	139
C12	149.1	153.0	139
C13	134.4	136.2	137
C14	132.3	134.0	124
C15	132.5	134.1	124
C16	133.8	135.9	129
C17	132.7	134.9	127
C18	132.0	134.1	126
C19	131.5	133.4	127
RMSD	**6.7**	**8.1**	

Note: [a]This work, [b]From SpectraBase, (n.a.) for benz in CHCl$_3$

An uninspected resulted is obtained because usually better correlations are observed with the 6-311++G** basis set than the other one due to that generate better-quality results for the ^{1}H nucleus than the C atoms. However, here similar RMSD values are predicted for the ^{1}H nucleus with the 6-31G* basis set and a lower value for the C atoms. Here, the similarity in the RMSD values for both H and C nucleuses support the presence of C2 in the liquid phase and probably also will be present in the solid state. Besides, these reasonable correlations suggest that the structures of C2 are optima to perform the vibrational studies with both methods.

Vibrational Study

In this analysis, we have considered the two C2 and C4 structures *s-Cis* experimentally observed for BENZ by X-ray diffraction at room temperature with the heating, respectively (Soares-Sobrinho, et al., 2008; Honorato, et al., 2014). Figures 8 and 9 show comparisons of

predicted IR and Raman spectra of C2 and C4 conformers of BENZ in ethanol and gas phase, respectively by using the B3LYP/6-311++G** method with the corresponding experimental Attenuated Total Reflectance Infrared (ATR-IR) and Raman spectra in the solid phase (Soares-Sobrinho, et al., 2010; SpectraBase, n.a.). We see reasonable concordances between the IR spectra of both forms in solution because the calculations in gas phase were performed for the isolated molecule where the forces packing were not considered while in solution the used method consider solute-solvent interactions and, hence, a higher number of bands are observed, as in the experimental spectrum.

Figure 8. Experimental ATR-IR Spectrum in the Solid State of BENZ Compared with the Corresponding Predicted for C2 and C4 Conformers in Ethanol Solution by Using B3LYP/6-311++G Level of Theory**
Source: SpectraBase, n.a.
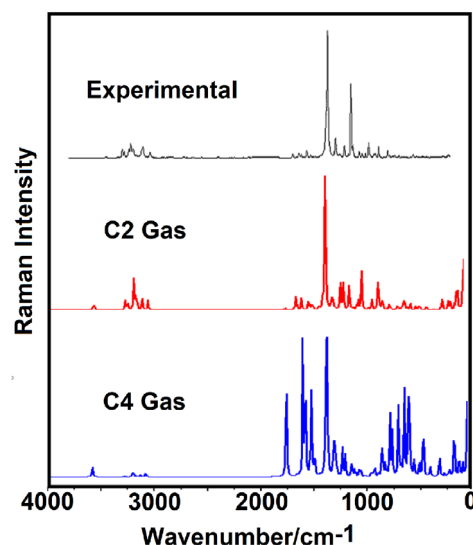
Figure 9. Experimental Raman Spectrum in the Solid State of BENZ Compared with the Corresponding Predicted for C2 and C4 Conformers in Ethanol Solution by Using B3LYP/6-311++G Level of Theory**
Source: Soares-Sobrinho, et al., 2010

Comparisons of both predicted Raman spectra with the corresponding experimental one after the conversion from scattering activities to Raman intensities by using known equations show very good correlations (Keresztury, et al., 1993). Optimized C2 and C4 conformers show C_1 symmetries and due to the 31 atoms present in both structures 87 normal vibration modes are expected for these species and, where all the vibration modes present activities in both spectra. Complete vibrational assignments have been performed using the SQMFF methodology and the Molvib program with potential energy distribution (PED) contributions ≥ 10%. In that procedure, normal internal coordinates and scaling factors were used (Pulay, et al., 1983; Rauhut, & Pulay, 1995; Sundius, 2002). Table 6 shows observed and calculated wavenumbers and assignments for C2 and C4 conformations of BENZ in gas phase using the B3LYP/6-311++G** level of theory. Here, the increasing in the intensities of IR and Raman bands between 1745-1503 cm^{-1} (Figure 9) are due to changes conformational, as mentioned by Honorate et al (2014). Hence, differences in the vibrational assignments and in the intensities of some IR and Raman bands for both IR spectra of C2 and C4 can be seen from Figs 8 and 9.

Experimental[c]		B3LYP 6-311++G** Method[a]			
		C2		C4	
IR	Raman	SQM[b]	Assignment[a]	SQM[b]	Assignment[a]
3330m	3261w	3424	νN5-H24	3415	νN5-H24
3180w		3135	νC13-H25	3134	νC13-H25
3160w	3157w	3113	νC16-H28	3112	νC16-H28
3120w	3115sh	3058	νC19-H31	3057	νC19-H31
3090w	3057sh	3048	νC18-H30	3048	νC14-H26
		3041	ν_aCH$_2$(C8)	3041	ν_aCH$_2$(C8)
		3040	νC19-H31,νC14-H26	3041	νC18-H30
	3029sh	3031	νC14-H26,νC17-H29	3032	νC17-H29
3000w	3015w	3024	νC15-H27	3022	νC15-H27
	2999vw	2984	ν_aCH$_2$(C8)	2989	ν_aCH$_2$(C9)
2949w	2941w	2980	ν_sCH$_2$(C8)	2979	ν_sCH$_2$(C8)
2894vw	2888sh	2927	ν_sCH$_2$(C9)	2934	ν_sCH$_2$(C9)
1685s	1657w	1680	νC10=O1	1680	νC10=O1
1685s	1657w	1591	νC14-C17	1590	νC14-C17
1565m	1583w	1572	νC18-C19	1571	νC18-C19,νC17-C19,νC11-C14, νC11-C15
1535s	1537w	1533	ν_aNO$_2$	1533	ν_aNO$_2$
1535s	1537w	1519	ν_aNO$_2$	1517	ρN5-H24
1480s	1503w	1480	ρN5-H24	1480	βC17-H29, βC18-H30
1478s		1471	βC17-H29	1471	νC13-C16
1465m		1457	νC13-C16	1457	νN6-C12,νN4-C12
1452m		1440	βC19-H31, βC18-H30	1440	βC19-H31,νC15-C18
1415w	1410sh	1419	δCH$_2$(C9)	1416	δCH$_2$(C9)
1415w	1381sh	1413	δCH$_2$(C8)	1412	δCH$_2$(C8)
1352vs	1359vs	1375	νN4-C13,νN6-C12,νN4-C12	1375	νN4-C13
		1367	wagCH$_2$(C9)	1365	wagCH$_2$(C9)
1336m	1330sh	1349	wagCH$_2$(C8)	1349	wagCH$_2$(C8)
1326sh	1300sh	1327	βC15-H27	1330	βC14-H26, βC15-H27
1287m	1288m	1323	ν_sNO$_2$	1322	ν_sNO$_2$
1287m	1253w	1320	νN7-C12	1319	νN7-C12,νN6-C12
1287m	1253w	1296	νC17-C19	1297	νC14-C17 ϱCH$_2$(C9)
		1263	νN4-C8,νN4-C12	1262	νN4-C8,νN4-C12
1248m		1245	νN5-C10,ρC10=O1	1245	νN5-C10
1211w	1212m	1228	ϱCH$_2$(C9),νC11-C15,νC11-C14	1227	ϱCH$_2$(C9),νC11-C14
	1178vw	1186	νC9-C11	1185	νC9-C11
		1181	ϱCH$_2$(C8)	1181	ϱCH$_2$(C8)
		1169	βC14-H26	1169	βC17-H29
1154s	1157vs	1155	νN6-C16	1155	νN6-C16
1139s	1139w	1149	βC19-H31,βC18-H30	1150	βC19-H31,βC18-H30
	1129sh	1100	N4-C13	1098	N4-C13,ϱCH$_2$(C8)
1080w	1088w	1070	νC15-C18	1071	νC15-C18
1057w	1064w	1064	βC13-H25,βC16-H28	1064	βC13-H25, βC16-H28
1028w	1034w	1025	νN5-C9	1022	νN5-C9
1028w	1034w	1021	βR$_1$(A1)	1020	βR$_1$(A1)

987w	1005m	996	γC19-H31	997	γC19-H31
987w	993sh	994	βR$_1$(A1),νC17-C19	994	βR$_1$(A1),νC17-C19
		978	γC18-H30	978	γC18-H30,γC14-H26
953w	956sh	974	τ$_w$CH$_2$(C9),νC8-C10	968	νC8-C10
944vw	946w	923	γC14-H26	926	γC15-H27
918m	918m	917	γC14-H26,βR$_2$(A2)	918	βR$_1$(A2), βR$_2$(A2)
906w		882	γC16-H28	881	γC16-H28
863vw	874vw	877	τ$_w$CH$_2$(C8)	877	τ$_w$CH$_2$(C8)
835s	839w	848	γC15-H27,γC17-H29	849	γC17-H29
835s	839w	844	δNO$_2$	844	δNO$_2$
822w	824w	829	wagC10=O1	831	wagC10=O1
		810	δN5C9C11	811	δN5C9C11
792sh	795w	799	τ$_w$CH$_2$(C9),νC8-C10	793	τ$_w$CH$_2$(C9)
778s	778w	780	γC13-H25	779	γC13-H25
744s	743w	752	τR$_1$(A1)	752	τR$_1$(A1),γC19-H31
744s	743w	738	wagNO$_2$	737	wagNO$_2$
694s	684vw	697	τR$_1$(A1)	695	τR$_1$(A1)
694s	684vw	675	νN4-C8	674	νN4-C8,ρC10=O1
683sh		640	τR$_2$(A2)	652	wagN5-H24
668vs		637	wag N5-H24,τR$_1$(A2)	640	τR$_2$(A2)
651sh	644vw	631	βR$_2$(A1),βR$_3$(A1)	631	βR$_2$(A1), βR$_3$(A1)
617m	620w	614	τR$_1$(A2)	616	τR$_1$(A2), wagN5-H24
595w	593vw	595	τR$_1$(A2),βR$_3$(A1)	605	τR$_1$(A2)
572sh	572vw	573	wag N5-H24,ρNO$_2$	569	ρNO$_2$, βC12-N7
558m	556vw	525	ρNO$_2$,wagC10=O1	527	ρNO$_2$
512w	509vw	494	τR$_2$(A1),γC11-C9	493	τR$_2$(A1),γC11-C9
468s	493vw	436	δN5-C10-C8	435	τR$_2$(A1), δN5-C10-C8
416w		429	νN7-C12,βN4-C8	431	νN7-C12
407sh		400	τR$_3$(A1)	399	τR$_3$(A1)
367w	368vw	372	βN4-C8,βC11-C9	359	βC11-C9
	319w	319	βC11-C9	320	βN4-C8
		306	βN4-C8,ρNO$_2$	292	βC12-N7
		254	βC12-N7	277	γC12-N7, δN4C8C10
		237	δC9-N5-C10	240	δC9-N5-C10
		200	γC12-N7,δN5-C10-C8	197	δN5-C10-C8
		176	γC12-N7	194	γC12-N7
		164	τC10-N5,wag N5-H24	156	τC10-N5,γC12-N7
		98	τwNO$_2$	105	τwNO$_2$
		83	τN4-C3,δN4C8C10	82	τN4-C3
		37	τC8-N4	48	τC8-C10
		32	τC10-N5,wag N5-H24	39	τC8-N4
		21	τwC11-C9	24	τC10-N5
		19	τC8-C10	18	τC8-N4τC10-N5
		4	τN5-C9	10	τN5-C9τwC11-C9

Note: Abbreviations: ν, stretching; β, deformation in the plane; γ, deformation out of plane; wag, wagging; τ, torsion; ρ, rocking; τw, twisting; δ, deformation; a, antisymmetric; s, symmetric; A1, Benzyl; A2, imidazole rings; [a]This work, [b]From SQMFF/B3LYP/6-311++G** method, [c]From SpectraBase, n.a.

Discussions on assignments of the most important groups are given below.

Band Assignments

NH modes. Generally, the NH stretching modes in compounds containing these groups are assigned between 3400 and 3300 cm^{-1} and, in the previous assignment reported by Soares-Sobrinho et al for BENZ this mode was assigned to the IR band at 3330 cm^{-1} (Soares-Sobrinho, et al., 2010; Karrouchi, et al., 2021; Karrouchi, et al., 2021; Mortada, et al., 2022). Hence, the IR band of medium intensity at 3330 cm^{-1} is without difficulty assigned to those vibration modes of C2 and C4, as observed in Table 6. The in-plane deformation or rocking mode are predicted by calculations for both conformers between 1517 and 1480 cm^{-1} (Soares-Sobrinho, et al., 2010; Karrouchi, et al., 2021; Karrouchi, et al., 2021; Mortada, et al., 2022). Hence, those modes are assigned accordingly. The SQM calculations predicted the out-of-plane deformation modes of C2 and C4 conformers coupled with other modes and between 652 and 573 cm^{-1}, hence; these modes are assigned to the shoulders at 683 and 572 cm^{-1}, as indicated in Table 6.

CH modes. In both conformers of BENZ there are seven aromatic C-H stretching modes (five of benzyl rings and two of imidazole rings). The SQM calculations predicted the stretching modes of imidazole rings between 3135 and 3112 cm^{-1}, hence; the IR bands between 3180 and 3160 cm^{-1} are assigned to those vibration modes, as expressed in Table 6. The C-H stretching modes of benzyl rings are predicted between 3058 and 3022 cm^{-1}, therefore, they are assigned in that mentioned region. The rocking modes for C2 and C4 conformers are predicted between 1480 and 1064 cm^{-1}, hence, they are assigned in these regions, as detailed in Table 6 (Karrouchi, et al., 2021; Laurella, et al., 2022; Karrouchi, et al., 2021; Mortada, et al., 2022). For both conformers the out-of-phase modes are assigned to the IR bands at 996 and 752 cm^{-1}, in accordance with the calculations (Karrouchi, et al., 2021; Laurella, et al., 2022; Karrouchi, et al., 2021; Mortada, et al., 2022; Ditchfield, 1974;

Romano, et al., 2013; Romano, Ladetto, & Brandán, 2013).

CH₂ modes. The positions of these groups in C2 is different from C4, as was observed by infrared spectroscopy by Honorate et al (2014). Thus, changes in the intensities of some bands between 1510 and 1400 cm^{-1} region are related to deformation modes of these groups predicted between 1415 and 1412 cm^{-1}. The SQM calculations predict the waging, rocking and twisting modes for these two conformers in approximately the same regions. Thus, the group of bands at 1367/1349, 1297/1181 and 974/793 cm^{-1} are assigned to those vibration modes.

NO₂ modes. Generally, the two NO₂ antisymmetric and symmetric stretching modes are assigned between 1584 and 1335 cm^{-1} (Romani, & Brandán, 2015; Castillo, et al., 2017). These N=O bonds in C2 and C4 conformers have double bond characters and, hence, the strong and medium intensity IR bands respectively at 1535 and 1287 cm^{-1} can easily be assigned to those modes for both conformers of BENZ. Normally, the NO₂ deformation modes are assigned between 841 and 821 cm^{-1} while the wagging modes of both forms are assigned at 775-756 cm^{-1}. In C2 and C4, the NO₂ deformation and wagging modes are predicted in the same region, hence, they were assigned to the weak band at 835 cm^{-1} and to the strong band at 744 cm^{-1}, respectively (Romani, & Brandán, 2015; Castillo, et al., 2017). The rocking modes are clearly predicted in the same region and, for this reason, those modes are assigned to the medium intensity IR band at 558 cm^{-1}, in accordance to those two tautomers which were assigned at 545 cm^{-1} (Romani, & Brandán, 2015). In those two thiol and thione tautomers, the twisting modes are predicted by SQM calculations between 66 and 63 cm^{-1} while for C2 and C4 these modes are predicted at 98 and 105 cm^{-1}, respectively (Romani, & Brandán, 2015; Castillo, et al., 2017). Obviously, due to the low wavenumbers values those modes were not assigned. This analysis shows clearly that the vibration modes related to these groups for C2 and C4 are predicted in the same region.

Skeletal modes. The C=O stretching modes of the two conformers together with the C=C of benzyl rings are predicted between 1680 and 1571 cm^{-1}, thus, the very strong IR band at 1685 and 1565 cm^{-1} are assigned to those stretching modes of both conformers. Besides, some N=C stretching modes of imidazole rings and acetamide fragment are predicted by the SQM/B3LYP/6-311++G** calculations with double bond character while other N-C and C-C stretching modes with partial double bond character, thus, the bands between 1478 and 1287 cm^{-1} can be assigned to those modes, as observed in similar species (Karrouchi, et al., 2021; Karrouchi, et al., 2021; Mortada, et al., 2022). However, the N-C and C-C stretching modes with simple bond character are assigned between 1248 and 694 cm^{-1}, as predicted by the SQM calculations and, as observed in Table 6. Note that the N7-C12 stretching modes of nitro groups linked to imidazole rings in C2 and C4 are assigned at 416 cm^{-1}, as predicted by calculations. The deformation and torsion modes of both benzyl and imidazole rings are predicted in approximately the same regions reported for other species (Karrouchi, et al., 2021; Karrouchi, et al., 2021; Mortada, et al., 2022; Sundius, & Brandán, 2023; Castillo, et al., 2018; Romano, E., et al., 2023; Romano, et al., 2011; Romano, et al., 2013; Romano, Ladetto, & Brandán, 2013; Romani, & Brandán, 2015; Castillo, et al., 2017) and, as a consequence they are clearly assigned in those regions. Assignments of the remaining skeletal modes expected for C2 and C4 conformers of BENZ are shown in Table 6.

Force Field

To characterize the force of different bonds, the scaled force constants are useful parameters associated to the positions of bands observed in the vibrational spectra. Hence, these factors for C2 and C4 of BENZ were computed in gas phase and ethanol solution at the B3LYP/6-311++G** level of theory by using the SQMFF methodology and the Molvib program (Pulay, et al., 1983; Rauhut, & Pulay, 1995; Sundius, 2002). These parameters for the two conformers in both media are shown in Table 7. Regarding the values of scaled force constants, we observed practically the same $f(\nu N\text{-}H)$, $f(\nu C\text{-}H)$ and $f(\nu C\text{=}O)$ force constants values for C2 and C4 in the two media, in agreement with the similar positions predicted by SQM calculations for the involved stretching modes. However, when the medium change from the gas phase to ethanol solution modifications in the $f(\nu C\text{-}N)$ and $f(\nu C\text{-}C)$ force constants values related to the acetamide fragments and to rings are observed. Such observations are associated to increase in the intensities of bands, as was aforementioned. Note that despite conformational changes between C2 and C4 the scaled $f(\nu CH_2)$ and $f(\nu NO_2)$ force constants present the same values in gas phase but slight decreasing in solution, as observed from Figs. 8 and 9.

Table 7. Comparison of Scaled Internal Force Constants for C2 and C4 Conformers of BENZ in Gas Phase and Ethanol Solution by Using the B3LYP/6311++G** Level of Theory

| Force constants | B3LYP/6311++G**[a] | | | |
| | C2 | | C4 | |
	Gas	Ethanol	Gas	Ethanol
$f(\nu N\text{-}H)$	6.50	6.50	6.50	6.50
$f(\nu C\text{-}H)_R$	5.16	5.17	5.14	5.17
$f(\nu C\text{-}N)_R$	6.62	6.60	6.62	6.58
$f(\nu C\text{-}C)_R$	6.44	6.37	6.51	6.36
$f(\nu CH_2)$	4.90	4.88	4.91	4.89
$f(\nu C\text{-}N)$	5.00	5.20	5.20	5.37

$f(\nu C\text{-}C)$	3.85	3.95	3.85	3.95
$f(\nu NO_2)$	9.15	8.60	9.15	8.55
$f(\nu C=O)$	11.00	10.10	11.00	10.1
$f(\delta C\text{-}C\text{-}N)$	1.15	1.28	1.23	1.33

Note: Units are mdyn Å^{-1} for stretching and mdyn Å rad^{-2} for angle deformations. ^{a}This work.

A very important observation is detected in the scaled $f(\square C\text{-}C\text{-}N)$ force constants related to the acetamide fragments because the values are different for both conformers in the two media. These variations are justified by the different $f(\nu C\text{-}N)$ and $f(\nu C\text{-}C)$ force constants values, as observed in Table 7.

Ultraviolet-Visible Spectrum

The electronic spectra for the C2 and C4 conformers of BENZ were predicted in ethanol solution at the B3LYP/6-311++G** and B3LYP/6-311G** levels of theory and both are compared in Figure 10. Different level of theory was used for C4 due to the difficulty to obtain the spectrum with the other method. The corresponding experimental obtained for BENZ in aqueous solution by Nothenberg et al (1991) showed two bands, one intense absorption at 203 nm and other of lower intensity at 314 nm while in the predicted spectra for C2 conformer the maximum appeared at 177 nm while the band of lower intensity at 307 nm. On the contrary, C4 shows a shoulder at 234 nm and a maximum at 285 nm. Thus, the spectrum of C2 shows a very good concordance with the experimental obtained in the solvent of higher polarity (water, 1.85 D) because both bands are located at higher wavelengths than the corresponding predicted in ethanol (1.66 D), for which, the observed hypsochromic shift is in agreement with the change in solvent polarity. Due to the presence of C=C, C=O and C=N double bonds these absorptions can be quickly assigned to $\pi \rightarrow \pi^*$ and $n \rightarrow \pi^*$ transitions, as reported for similar compounds and as suggested by NBO calculations (Nogueira Silva, et al., 2008; Honorato, et al., 2014; Nothenberg, Funayama, & Najjar, 1991).
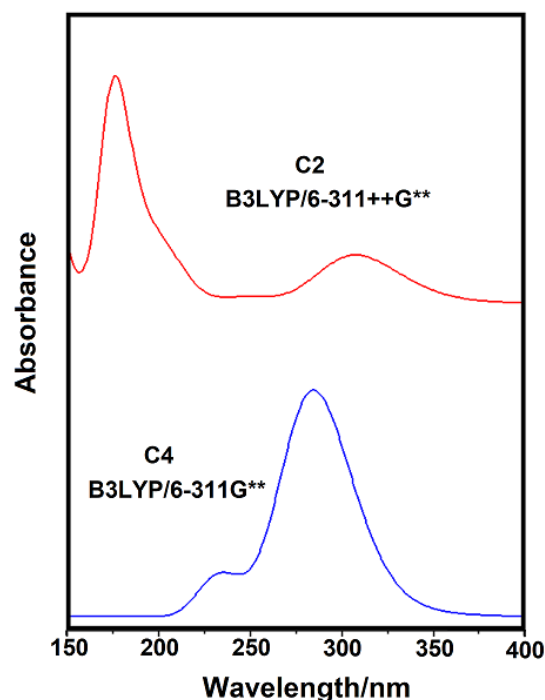
Figure 10. Predicted Electronic Spectra for C2 and C4 of BENZ in Ethanol Solution at the B3LYP/6-311++G Level of Theory**

On the other side, the bands associated to nitrate groups are expected between 208 and 214 nm and, where the intense band predicted at 203 nm overlaps the bands. The differences observed with C4 are justified by the different method and solvent used.

Conclusions

In this work, two C2 and C4 stable *cis* conformers of benznidazole active drug used to the treatment of Chagas disease have been theoretically characterized and its vibrational spectra completely assigned combining B3LYP/6-311++G** calculations with the

experimental FT-IR and FT-Raman spectra and the SQMFF methodology. Both forms were experimentally determined by X-ray diffraction and they differ in the positions of the CH_2 groups linked to benzyl and imidazole rings. C2 was observed at room temperature while C4 with the heating. Changes in the positions, directions and orientations of dipole moments vectors and in the magnitudes could explain the presence of C2 in the solid phase. The mapped MEP surfaces show that the nucleophilic regions are located on N6 of imidazole ring and on the O atoms of NO_2 and on C=O groups while the electrophilic sites are observed on the N-H and CH_2 groups of acetamide fragment.

The NBO studies show that C2 is most stable in solution and that the E values are strongly dependent on method and basis set. The AIM analyses reveal the high stability of C2 in the gas phase and in ethanol solution, as supported by the different N-H···O, C-H···O and C-O···H interactions of H bonds. Besides, both studies reveal the influence of level of theory and the medium on the total stabilization energy.

The low gap value and the high reactivity of C2 could explain their biological activities.

Reasonable concordances were found among the experimental FTIR, FT-Raman, UV-Visible and ^{1}H and ^{13}C-NMR spectra and their corresponding theoretical ones. Complete vibrational assignments of the 87 normal vibration modes for both conformers of BENZ were reported for first time together with the scaled force constants for C2 and C4 conformers.

Supporting Information Available

Tables S1-S3 and Figures S1-S3 in the Appendixes 1,2.

Acknowledgements

The authors would like to thank Prof. Tom Sundius for his permission to use MOLVIB.

Author contribution

Funding

Data Availability

Available when the authors require it.

Conflicts of Interest

The authors declare no conflict of interest.

References

Aguirre, G., Boiani, L., Cerecetto, H., Fernández, M., González, M., Denicola, A., Otero, L., Gambino, D., Rigol, C., Olea-Azar, C., & Faundez, M. (2004). In vitro activity and mechanism of action against the protozoan parasite Trypanosoma cruzi of 5-nitrofuryl containing thiosemicarbazones. *Bioorganic & medicinal chemistry*, *12*(18), 4885–4893. https://doi.org/10.1016/j.bmc.2004.07.003

Arancibia, R., Klahn, H., Buono-Core, G., & Garland, M.T. (2013). Organometallic Scchiff bases derived from 5-nitrophiophene and 5-nitrofurane: Synthesis, crystallographic, electrochemical, ESR and antitrypanosoma cruzi studies. *Journal of Organometallic chemistry*, *743*, 49-54. https://doi.org/10.1016/j.jorganchem.2013.06.014

Arenas Velásquez, A.M., Francisco, A.I., Nakaima Kohatsu, A.A., Alves de Jesus, S. F., Rodrigues, D.F., Gomes da Silva, T. R., Galdorfini Chiari, B., De Almeida, M.G.J.,

Borges Isaac, V.L., Vargas, M.D., & Barretto Cicarelli, R.M. (2014). Synthesis and tripanocidal activity of ferrocenyl and benzyl diamines against Trypanosoma brucei and Trypanosoma cruzi. *Bioorganic & Medicinal Chemistry Letters, 24,* 1707–1710. https://doi.org/10.1016/j.bmcl.2014.02.046

Bader, R.F.W. (1990). *Atoms in Molecules. A Quantum Theory.* Oxford: Oxford University Press.

Becke, A.D. (1988). Density-functional exchange-energy approximation with correct asymptotic behavior. *Physical Review A, 38,* 3098-3100. https://doi.org/10.1103/physreva.38.3098

Bern, C. (2015). Chagas disease. *New England Journal of Medicine, 373,* 456–466. https://doi.org/10.1056/nejmc15109964

Besler, B.H., Merz, Jr K.M., & Kollman P.A. (1990). Atomic charges derived from semiempirical methods. *Journal of Computational Chemistry, 11,* 431-439. https://doi.org/10.1002/jcc.540110404

Bezerra, E. M., Bezerra-Neto, J. R., Sales, F. A., dos Santos, R. P., Martins, A. M., de Lima-Neto, P., Caetano, E. W., Albuquerque, E. L., & Freire, V. N. (2014). Optical absorption of the antitrypanocidal drug benznidazole in water. *Molecules (Basel, Switzerland), 19*(4), 4145–4156. https://doi.org/10.3390/molecules19044145

Biegler-Köning, F., Schönbohm, J., & Bayles, D. (2001). AIM2000; A Program to Analyze and Visualize Atoms in Molecules. *Journal of Computational Chemistry, 22* 545. https://doi.org/10.1002/1096-987X(20010415)22:5<545::AID-JCC1027>3.0.CO;2-Y

Caryn, B. (2015). Chagas disease in Latin America: an epidemiological update based on 2010 estimates. *Weekly Epidemiological Record, 90,* 33–44. https://doi.org/10.1056/nejmra1410150

Castillo, M.V., Iramain, M.A., Davies, L., Manzur, M.E., & Brandán, S.A. (2018). Evaluation of the structural properties of powerful pesticide dieldrin in different media and their complete vibrational assignment. *Journal of Molecular Structure, 1154,* 392-405. https://doi.org/10.1016/j.molstruc.2017.10.065.

Castillo, M.V., Rudyk, R.A., Davies, L., & Brandan, S.A. (2017). Analysis of the structure and the FT-IR and Raman spectra of 2-(4-nitrophenyl)-4H-3,1-benzoxazin-4-one. Comparisons with the chlorinated and methylated derivatives. *Journal of Molecular Structure, 1140,* 2-11. http://dx.doi.org/10.1016/j.molstruc.2016.08.070

Chai, J.-D. & Head-Gordon, M. (2018). Long-range corrected hybrid density functionals with damped atom-atom dispersion corrections. *Physical chemistry, chemical physics, 10,* 6615-6620. https://doi.org/10.1039/B810189B

Dennington, R.D., Keith, T.A. & Millam, J.M. (2019). *GaussView, version 6.1.1.* Semichem Inc., Shawnee Mission, KS.

Ditchfield, R. (1974). Self-consistent perturbation theory of diamagnetism. I. A gage-invariant LCAO (linear combination of atomic orbitals) method for NMR chemical shifts, *Journal of Molecular Structure, 27,* 714–722. https://doi.org/10.1080/00268977400100711

Figueirêdo, C. B. M., Nadvorny, D., de Medeiros Vieira, A. C. Q., Soares Sobrinho, J. L., Rolim Neto, P. J., Lee, P. I., & de La Roca Soares, M. F. (2017). Enhancement of dissolution rate through eutectic mixture and solid solution of posaconazole and benznidazole. *International journal of pharmaceutics, 525*(1), 32–42. https://doi.org/10.1016/j.ijpharm.2017.04.021

Figueroa, R., Norambuena, E., Olea-Azar, C., Aguirre, G., Cerecetto, H., González, M., Morello, A., Maya, J.D., Garatf, B., & Gambino, D. (2018). Platinum(II) metal complexes as potential anti-Trypanosoma cruzi agents. *Journal of Inorganic Biochemistry, 102,* 1033–1043. https://doi.org/10.1016/j.jinorgbio.2007.12.005

Frisch, M.J., Trucks, G.W., Schlegel, H.B. & Scuseria, G.E. (2019). *Gaussian 16, Revision C.01.* Wallingford CT.

Glendening, E.D., Badenhoop, J.K., Reed, A.D., Carpenter, J.E., & Weinhold, F. (1996). *NBO 3.1*. Theoretical Chemistry Institute. University of Wisconsin; Madison, WI.

Guzzetti K., Brizuela A.B., Romano E., Brandán S.A. (2013). Structural and vibrational study on zwitterions of L-threonine in aqueous phase using the FT-Raman and SCRF calculations. *Journal of Molecular Structure, 1045*, 171-179. https://doi.org/10.1016/j.molstruc.2013.04.016

Honorato, S. B., Mendonça, J. S., Boechat, N., Oliveira, A. C., Mendes Filho, J., Ellena, J., & Ayala, A. P. (2014). Novel polymorphs of the anti-Trypanosoma cruzi drug benznidazole. *Spectrochimica acta. Part A, Molecular and biomolecular spectroscopy, 118*, 389–394. https://doi.org/10.1016/j.saa.2013.08.096

Karrouchi, K., Brandán, S.A., Hassan, M., Bougrin, K., Radi, S., Ferbinteanu, M., Garcia, Y., & Ansar, M. (2021). Synthesis, X-ray, spectroscopy, molecular docking and DFT calculations of (*E*)-*N'*-(2,4-dichlorobenzylidene)-5-phenyl-*1H*-pyrazole-3-carbohydrazide. *Journal of Molecular Structure, 1228*, 129714. https://doi.org/10.1016/j.molstruc.2020.129714

Karrouchi, K., Brandán, S.A., Sert, Y., El Karbane, M., Radi, S., Ferbinteanu, M., Garcia, Y., & Ansar, M. (2021). Synthesis, structural, molecular docking and spectroscopic studies of (E)-N'-(4-methoxybenzylidene)-5-methyl-1H-pyrazole-3-carbohydrazide. *Journal of Molecular Structure, 1225,* 129072. https://doi.org/10.1016/j.molstruc.2020.129072

Keresztury, G., Holly, S., Besenyei, G., Varga, J., Wang, A.Y. & During, J.R. (1993). Vibrational spectra of monothiocarbamates-II. IR and Raman spectra, vibrational assignment, conformational analysis and *ab initio* calculations of *S*-methyl-*N,N*-dimethylthiocarbamateSpectrochim. *Spectrochimica Acta Part A: Molecular Spectroscopy, 49A*, 2007-2026.

https://doi.org/10.1016/S0584-8539(09)91012-1

Laurella, L.C., Ruiz Hidalgo, J., Catalán, C.A.N., Sülsen, V.P., & Brandán, S.A. (2022). Structure and absolute configuration of parodiolide, a new dimeric sesquiterpene lactone isolated from Mikania parodii Cabrera possessing an uncommon spiro connexion. *Journal of Molecular Structure, 1253*, 132270. https://doi.org/10.1016/j.molstruc.2021.132270

Lee, C., Yang, W. & Parr, R.G. (1988). Development of the Colle-Salvetti correlationenergy formula into a functional of the electron density. *Physical Review B, 37*, 785-789. https://doi.org/10.1103/physrevb.37.78

Marenich, A.V., Cramer, C.J. & Truhlar, D.G. (2009). Universal solvation model based on solute electron density and a continuum model of the solvent defined by the bulk dielectric constant and atomic surface tensions. *Journal of Physical Chemistry, B113*, 6378-6396. https://doi.org/10.1021/jp810292n

Miertus, S., Scrocco, E. & Tomasi, J. (1981). Electrostatic interaction of a solute with a continuum. *Chemical Physics, 55,* 117-129. https://doi.org/10.1016/0301-0104(81)85090-2

Morillo, C. A., Waskin, H., Sosa-Estani, S., Del Carmen Bangher, M., Cuneo, C., Milesi, R., Mallagray, M., Apt, W., Beloscar, J., Gascon, J., Molina, I., Echeverria, L. E., Colombo, H., Perez-Molina, J. A., Wyss, F., Meeks, B., Bonilla, L. R., Gao, P., Wei, B., McCarthy, M., … STOP-CHAGAS Investigators (2017). Benznidazole and Posaconazole in Eliminating Parasites in Asymptomatic T. Cruzi Carriers: The STOP-CHAGAS Trial. *Journal of the American College of Cardiology, 69*(8), 939–947. https://doi.org/10.1016/j.jacc.2016.12.023

Mortada, S., Brandán, S.A., Karrouchi, K., El-guourrami, O., Doudach, L., El Bacha, R., Ansar, M., & El Abbes Faouzi, M. (2022). Synthesis, spectroscopic and DFT studies of 5-methyl-*1H*-pyrazole-3-carbohydrazide N-glycoside as potential anti-diabetic and antioxidant agent. *Journal of Molecular Structure.*

1267, 133652. https://doi.org/10.1016/j.molstruc.2022.133652

Nogueira Silva, J.J., Pavanelli, W.R., Gutierrez, F.R., Alves Lima, F.C., Ferreira da Silva, A.B., Santana Silva, J., & Wagner Franco, D. (2008). Complexation of the anti-Trypanosoma cruzi drug benznidazole improves solubility and efficacy. *Journal of medicinal chemistry*, *51*(14), 4104–4114. https://doi.org/10.1021/jm701306r

Nothenberg, M.S., Funayama, G.K., & Najjar, R. (1991). Adducts of Nitroimidazole Derivatives With Rhodium(II) Carboxylates: Syntheses, Characterization, and Evaluation of Antichagasic Activities. *Journal of Inorganic Biochemistry*, *42*, 217-229. https://doi.org/10.1016/0162-0134(91)84008-w

Olivera, B.G., Alencar, Filho E.B. & Vasconcellos, M.L.A.A. (2016). Comparisons between Crystallografy Data and Theoretical Parameters and the Formation of Intramolecular Hydrogen Bonds: Benznidazole. *Crystals, 6*(56), 1-11. https://doi.org/10.3390/cryst6050056

Parr, R.G. & Pearson, R.G. (1983). Absolute hardness: companion parameter to absolute electronegativity. *Journal of American Chemical Society*, *105,* 7512-7516. https://doi.org/10.1021/ja00364a005.

Pires, M.F., De Paula, L.M., Figueiredo, V.P., Mayer de Andrade, I., Talvani, A., Sá-Barreto, L.C., Bahia, M.T., & Cunha-Filho, M.S.S. (2011). Benznidazole microcrystal preparation by solvent change precipitation and in vivo evaluation in the treatment of Chagas disease, *European Journal of Pharmaceutics and Biopharmaceutics, 78,* 377–384. https://doi.org/10.1016/j.ejpb.2011.03.003

Pires, M.F., Hideki Yoshizane, C.G., & Souza J. (2010). Caracterizaçao Fisico-Quimica do Farmaco antichagásico Benznidazol. *Quim Nova. 33*(8), 1714-1719. https://doi.org/10.1590/S0100-40422010000800018.

Pulay P., Fogarasi, G., Pongor, G., Boggs, J.E. & Vargha, A. (1983). Combination of theoretical ab initio and experimental information to obtain reliable harmonic force constants. Scaled quantum mechanical (QM) force fields for glyoxal, acrolein, butadiene, formaldehyde, and ethylene. *Journal of American Chemical Society*, 105, 7073. https://doi.org/10.1021/ja00362a005

Rassi, A.Jr., Rassi, A., & Marin-Neto, J.A. (2010). Chagas disease. *Lancet, 375*, 1388–1402. https://doi.org/10.1016/s0140-6736(10)60061-x

Rauhut, G. & Pulay, P. (1995). Transferable scaling factors for density functional derived vibrational force fields. J*ournal of Physical Chemistry, 99,* 3093–3099. https://doi.org/10.1021/j100010a019

Romani D. and Brandán S. A. Structural (2015). Spectroscopic studies of two 1,3-benzothiazole tautomers with potential antimicrobial activity in different media. Prediction of their reactivities. *Computational and Theoretical Chemistry, 1061,* 89-99. https://doi.org/10.1016/j.comptc.2015.03.018

Romano, E., Castillo, M.V., Pergomet, J., Zinczuk, J. & Brandán, S.A. (2013). Synthesis, Structural Study and Spectroscopic Characterization of a Quinolin-8-Yloxy Derivative with Potential Biological Properties. *Journal of Synthesis Theory and Applications*, *2*, 8-22. https://doi.org/10.4236/ojsta.2013.21002

Romano, E., Ladetto, F., & Brandán, S.A. (2013). Structural and vibrational studies of the potential anticancer agent, 5-difluoromethyl-1,3,4-thiadiazole-2-amino by DFT calculations. *Computational & Theoretical Chemistry, 1011*, 57-64. https://doi.org/10.1016/j.comptc.2013.01.016

Romano, E., Manzur, M.E., Iramain, M.A., & Brandán S.A. (2023). Effect of long-range corrections on Intermolecular interactions and Vibrational assignments of Ethylene Oxide Dimer. A Combined DFT and SQFF Study. *The International Journal of Engineering & Science.*

Romano, E., Raschi, A.B., Benavente, A.M., & Brandán, S.A. (2011). Structural analysis, vibracional spectra and coordinated normal of 2R-(-)-6-hydroxytremetone. *Spectrochimica Acta Part A*: *Molecular and Biomolecular Spectroscopy, 84*,

111-116.
https://doi.org/10.1016/j.saa.2011.09.011

Soares-Sobrinho, J. L., de La Roca Soares, M. F., Lopes, P. Q., Correia, L. P., de Souza, F. S., Macêdo, R. O., & Rolim-Neto, P. J. (2010). A preformulation study of a new medicine for Chagas disease treatment: physicochemical characterization, thermal stability, and compatibility of benznidazole. *AAPS PharmSciTech*, *11*(3), 1391–1396. https://doi.org/10.1208/s12249-010-9495-8

Soares-Sobrinho, J. L., Santos, F. L., Lyra, M. A., Alves, L. D., Rolim, L. A., Lima, A. A., Nunes, L. C., Soares, M. F., Rolim-Neto, P. J., & Torres-Labandeira, J. J. (2012). Benznidazole drug delivery by binary and multicomponent inclusion complexes using cyclodextrins and polymers. *Carbohydrate polymers*, *89*(2), 323–330. https://doi.org/10.1016/j.carbpol.2012.02.042

Soares-Sobrinho, J.L., Cunha-Filho, M.S.S., Rolim Neto, P.J., Torres-Labandeira, J.J., & Dacunha-Marinho, B. (2008). Benznidazole. *Acta Crystallographica Section A, E64*, o634. https://doi.org/10.1107/S1600536808005023

SpectraBase. (n.a.). Online Spectral Database: Quick access to millions of NMR, IR, Raman, UV-Vis, and Mass Spectra. Retrieved from https://spectrabase.com/spectrum

Streck, L., Sarmento, V. H., Machado, P. R., Farias, K. J., Fernandes-Pedrosa, M. F., & da Silva-Júnior, A. A. (2016). Phase Transitions of Isotropic to Anisotropic Biocompatible Lipid-Based Drug Delivery Systems Overcoming Insoluble Benznidazole Loading. *International journal of molecular sciences*, *17*(7), 981. https://doi.org/10.3390/ijms17070981

Sundius, T. (2002). Scaling of ab initio force fields by MOLVIB. V*ibrational Spectroscopy, 29,* 89-95. https://doi.org/10.1016/S0924-2031(01)00189-8

Sundius, T., & Brandán, S.A. (2023). Structural, harmonic force field and vibrational studies of cholinesterase inhibitor tacrine used for treatment of Alzheimer's disease. *Heliyon*, *9*, e17280.
https://doi.org/10.1016/j.heliyon.2023.e17280.

Tomasi, J., & Persico, J. (1994). Molecular Interactions in Solution: An Overview of Methods Based on Continous Distributions of the Solvent. *Chemical Review*, *94*, 2027-2094. https://doi.org/10.1021/cr00031a013.

Tonin, L.T., Barbosa, V.A., Bocca, C.C., Ramos, E.R., Nakamura, C.V., Da Costa, W.F., Basso, E.A., Nakamura, T.U., & Sarragiotto, M.H. (2009). Comparative study of the trypanocidal activity of the methyl 1-nitrophenyl-1,2,3,4-9H-tetrahydro-beta-carboline-3-carboxylate derivatives and benznidazole using theoretical calculations and cyclic voltammetry. *European Journal of Medicinal Chemistry, 44*(4), 1745-1750. https://doi.org/10.1128/AAC.03340-14

Trochine, A., Creek, D. J., Faral-Tello, P., Barrett, M. P., & Robello, C. (2014). Benznidazole biotransformation and multiple targets in Trypanosoma cruzi revealed by metabolomics. *PLoS neglected tropical diseases*, *8*(5), e2844.
https://doi.org/10.1371/journal.pntd.0002844

C4 Gas Phase
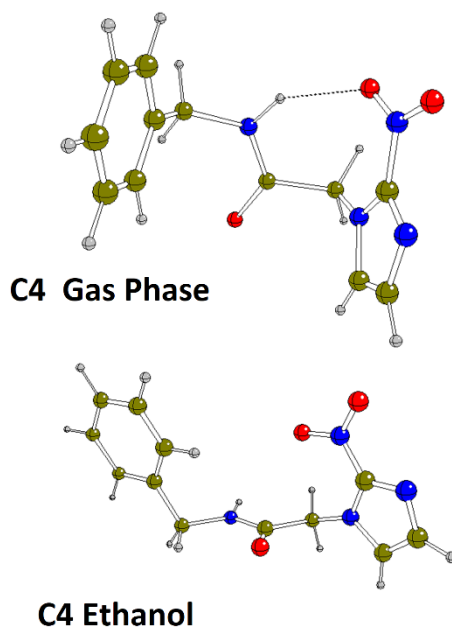
C4 Ethanol

Figure S1. Molecular Structures of C4 Conformer of Benznidazole in Gas Phase and Ethanol Solution by Using the B3LYP/6-311++G Method**
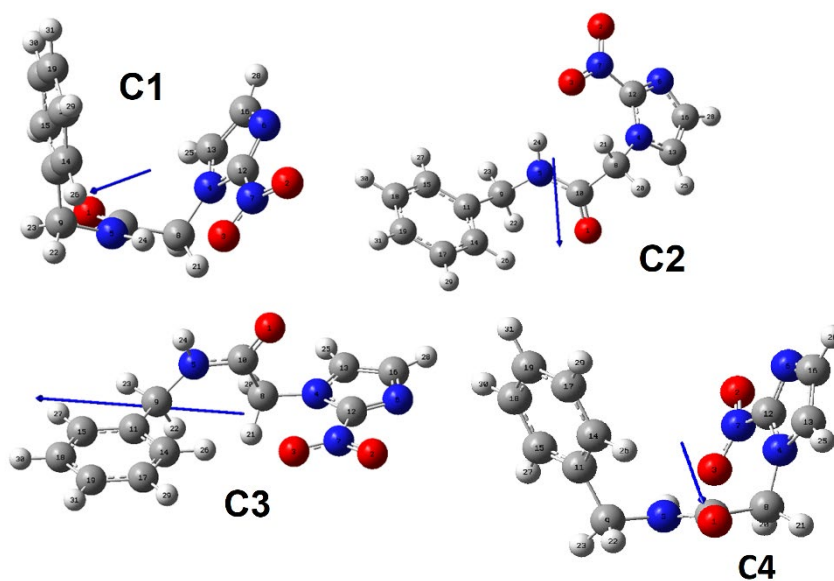
Figure S2. Positions and orientations of dipole moment vectors for the four conformers of BENZ in gas phase by using the B3LYP/6-311++G level of theory.**

Figure S3. Comparison Between the Theoretical Molecular Structures of 6-nitro-1,3-benzothiazole-2(3H)-thione and Their Tautomer 6-nitro-1,3-benzothiazole-2-thiol by Using the B3LYP/6-31G* Level of Theory

**Table S1. Main Delocalization Energies (in kJ/mol)
for C2 Conformer of BENZ in Gas Phase and Ethanol
Solution by Using Two Levels of Theory**

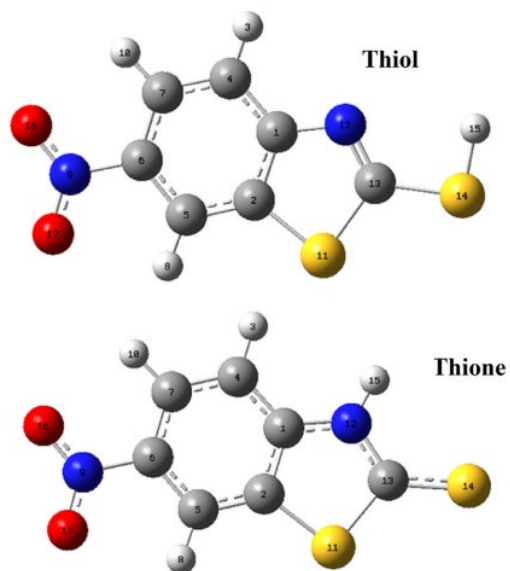| Delocalization	B3LYP/6-31G*		B3LYP/6-311++G**	
	Gas	PCM	Gas	PCM
$\pi O2\text{-}N7 \rightarrow LP(3)O3$		44.77		44.98
$\pi N4\text{-}C12 \rightarrow LP(2)N6$				78.62
$\pi C13\text{-}C16 \rightarrow LP(2)N6$				343.76
$\Sigma\Delta E_{\pi \rightarrow LP}$		**44.77**		**467.36**
$\pi N4\text{-}C12 \rightarrow \pi^*O2\text{-}N7$				46.52
$\pi N4\text{-}C12 \rightarrow \pi^*C13\text{-}C16$				75.45
$\pi N6\text{-}C12 \rightarrow \pi^*O2\text{-}N7$	69.73	80.67	66.59	
$\pi N6\text{-}C12 \rightarrow \pi^*C13\text{-}C16$	87.36	85.44	85.94	
$\pi C11\text{-}C15 \rightarrow \pi^*C14\text{-}C17$	81.38	82.30	81.80	82.79
$\pi C11\text{-}C15 \rightarrow \pi^*C18\text{-}C19$	84.39	85.40	84.48	86.15
$\pi C13\text{-}C16 \rightarrow \pi^*N6\text{-}C12$	78.75	84.23	79.80	56.85
$\pi C14\text{-}C17 \rightarrow \pi^*C11\text{-}C15$	86.23	85.31	87.85	86.86
$\pi C14\text{-}C17 \rightarrow \pi^*C18\text{-}C19$	84.48	83.43	84.23	83.72
$\pi C18\text{-}C19 \rightarrow \pi^*C11\text{-}C15$	83.43	82.89	83.52	82.42
$\pi C18\text{-}C19 \rightarrow \pi^*C14\text{-}C15$	82.68	83.93	83.10	84.06
$\Sigma\Delta E_{\pi \rightarrow \pi^*}$	**738.43**	**753.53**	**737.31**	**684.82**
$LP(2)O1 \rightarrow \sigma^*N5\text{-}C10$	99.86	94.43	86.14	89.08
$LP(2)O1 \rightarrow \sigma^*C8\text{-}C10$	94.84	90.00	88.41	82.89
$LP(2)O2 \rightarrow \sigma^*O3\text{-}N7$	85.02	78.83	84.35	77.41
$LP(2)O2 \rightarrow \sigma^*N7\text{-}C12$	57.85	50.08	56.81	47.02
$LP(2)O3 \rightarrow \sigma^*O2\text{-}N7$	78.67	78.75	74.32	78.58
$LP(2)O3 \rightarrow \sigma^* O2\text{-}N7$		41.80		612.24
$LP(1)N6 \rightarrow \sigma^*N4\text{-}C12$	45.94	43.97	43.97	
$LP(1)N5 \rightarrow \sigma^*O1\text{-}C10$				306.56
$\Sigma\Delta E_{LP \rightarrow \sigma^*}$	**462.18**	**507.87**	**390.03**	**1293.78**
$LP(3)O3 \rightarrow \pi^*O2\text{-}N7$	528.23	608.15	531.36	612.24
$LP(1)N4 \rightarrow \pi^*N6\text{-}C12$	202.14	219.74	196.21	
$LP(1)N4 \rightarrow \pi^*C13\text{-}C16$	142.12	149.14	138.52	
$LP(1)N5 \rightarrow \pi^*O1\text{-}C10$	315.17	328.00	299.79	306.56
$LP(1)N6 \rightarrow \pi^*N4\text{-}C12$				724.60
$LP(1)N6 \rightarrow \pi^*C13\text{-}C16$				191.28
$\Sigma\Delta E_{LP \rightarrow \pi^*}$	**1187.66**	**1107.03**	**1165.88**	**1834.00**
$\pi^*O2\text{-}N7 \rightarrow \pi^*N6\text{-}C12$	125.65	141.24	115.41	
$\pi^*O2\text{-}N7 \rightarrow \pi^*N4\text{-}C12$				299.7
$\pi^* N6\text{-}C12 \rightarrow \pi^*C13\text{-}C16$	386.65	265.51	377.24	103.54
$\Sigma\Delta E_{\pi^* \rightarrow \pi^*}$	**512.30**	**406.75**	**492.65**	**403.24**
$\Sigma\Delta E_{TOTAL}$	**2900.57**	**2819.95**	**2785.87**	**4683.20**

Note: [a]This work

Table S2. Analysis of the Bond Critical Points (BCP) and Ring Critical Points (RCP) for BENZ in Gas Phase and Ethanol Solution by Using Two Levels of Theory

Parameter[#]	B3LYP/6-31G*															
	Gas								Ethanol							
	RCPA1	RCPA2	RCPN1	RCPN2	RCPN3	O1-H26	O3-H24	O3-H21	RCPA1	RCPA2	RCPN1	RCPN2	RCPN3	O1-H26	O3-C8	O3-H21
$\rho(r)$	0.0200	0.0542	0.0047	0.0089	0.0128	0.0053	0.0200	0.0175	0.0202	0.0543			0.0131		0.0147	
$\nabla^2\rho(r)$	0.1616	0.4231	0.0200	0.0426	0.0625	0.0199	0.0656	0.0644	0.1620	0.4255			0.0639		0.0585	
$\lambda1$	-0.0149	-0.0628	-0.0016	-0.0057	-0.0090	-0.0042	-0.0252	-0.0187	-0.0149	-0.0631			-0.0095		-0.0112	
$\lambda2$	0.0861	0.2399	0.0050	0.0205	0.0162	-0.0034	-0.0234	-0.0134	0.0859	0.2416			0.0126		-0.0066	
$\lambda3$	0.0904	0.2459	0.0165	0.0278	0.0553	0.0275	0.1143	0.0965	0.0909	0.2470			0.0607		0.0764	
$|\lambda1|/\lambda3$	0.1648	0.2553	0.0969	0.2050	0.1627	0.1527	0.2204	0.1938	0.1540	0.2555			0.1565		0.1466	
Distances						2.790	2.082	2.270								
Parameter[#]	B3LYP/6-311++G**															
	Gas								Ethanol							
	RCPA1	RCPA2	RCPN1	RCPN2	RCPN3	O1-H26	O3-H24	O3-H21	RCPA1	RCPA2	RCPN1	RCPN2	RCPN3	O1-H26	O3-C8	O3-H21
$\rho(r)$	0.0217	0.0576		0.0091	0.0131		0.0171	0.0173	0.0218	0.0576			0.0129		0.0141	
$\nabla^2\rho(r)$	0.1596	0.3981		0.0404	0.0634		0.0638	0.0633	0.1597	0.4016			0.0618		0.0558	
$\lambda1$	-0.0168	-0.0653		-0.0057	-0.0094		-0.0196	-0.0178	-0.0167	-0.0655			-0.0089		-0.0105	
$\lambda2$	0.0863	0.2237		0.0206	0.0169		-0.0189	-0.0131	0.0860	0.2252			0.0111		-0.0064	
$\lambda3$	0.0903	0.2398		0.0255	0.0560		0.1024	0.0943	0.0906	0.2407			0.0597		0.0728	
$|\lambda1|/\lambda3$	0.1860	0.2723		0.2235	0.1678		0.1914	0.1888	0.1843	0.2721			0.1491		0.1442	
Distances							2.123	2.282								

Note: RCPA1 (Six member) RCPA2 (Five member)

Table S3. The Frontier Molecular HOMO and LUMO Orbitals and Some Descriptors for the BENZ in Gas phase by Using Two Levels of Theory

Orbital (eV)	BENZ[a]				B3LYP/6-31G*	
	B3LYP/6-31G*		B3LYP/6311++G**		thione[b]	thiol[b]
	Gas	Ethanol	Gas	Ethanol	Gas	Gas
HOMO	-6.6993	-6.5834	-7.1044	-6.8816	-6.4443	-6.8847
LUMO	-2.8221	-2.7240	-3.2288	-3.2008	-2.7918	-2.6194
|GAP|	3.8772	3.8594	3.8756	3.6808	3.6525	4.2653
Descriptors						
(eV)	Gas	PCM	Gas	PCM		
χ	-1.9386	-1.9297	-1.9378	-1.8404	-1.8263	-2.1327
μ	-4.7607	-4.6537	-5.1666	-5.0412	-4.6180	-4.7521
η	1.9386	1.9438	1.9438	1.8404	1.8263	2.1327
S	0.2579	0.2572	0.2572	0.2717	0.2738	0.2345
ω	5.8456	5.5706	6.8662	6.9043	5.8388	5.2943

Note: [a]This work, [b]From Romani, & Brandán, 2015. $\chi = -[E(LUMO)- E(HOMO)]/2$; $\mu = [E(LUMO) + E(HOMO)]/2$; $\eta = [E(LUMO) - E(HOMO)]/2$; $S = \frac{1}{2}\eta$; $\omega = \mu^2/2\eta$